Journal of Engineering Science and Technology Review 17 (2) (2024) 58 - 65

Research Article

JOURNAL OF
Engineering Science and Technology Review

www.jestr.org

Working Condition Identification Method for the Scarifying Tooth Harrow Monitoring System of a Roller-type Residual Film Collector

Dangqin Xue[1,*], Xiaodong Zhang[2], ZhaoSen Dong[3], Jiaxi Zhang[3] and Huojie Shi[4]

[1]*Nanyang Institute of Technology, Nanyang 473000, China*
[2]*College of Automation Engineering, Henan Polytechnic Institute, Nanyang 473000, China*
[3]*Mechanical and Electrical Engineering Institute, Xinjiang Agricultural University, Urumqi 830052, China*
[4]*Department of Biological Systems Engineering, Washington State University, Pullman, MI 98101, United States*

Received 19 January 2024; Accepted 31 March 2024

Abstract

The roller-type residual film collector is the main machine type for collecting residual films. The scarifying tooth harrow bears the largest resistance among all the components of the entire machine, and it directly affects the quality and efficiency of the residual film collector. In this study, the arithmetic optimization algorithm- variational mode decomposition - bidirectional long short-term memory (AOA-VMD-BiLSTM) model was proposed to improve the working condition identification accuracy of the scarifying tooth harrow. First, the locations of three scarifying tooth harrow monitoring points were analyzed, the arithmetic optimization algorithm was introduced to optimize the variational mode decomposition (VMD) parameters, and the optimal parameter combination of the three monitoring points was acquired. Second, the reconstructed signal for the three monitoring points on the scarifying tooth harrow after VMD decomposition was subjected to two-way updating and recursion with bidirectional long short-term memory (BiLSTM) as the core of the model, and iterative training of the scarifying tooth harrow under four working conditions was performed. Last, the new sample set and the original dataset were imported into two deep learning models, namely, BiLSTM and long short-term memory (LSTM), followed by a comparative validation of the training results of VMD-BiLSTM, VMD-LSTM, BiLSTM, and LSTM models. Results demonstrate that among the models, VMD-BiLSTM exerts the best processing effect on complex signals and has a higher convergence rate, better convergence stability, and higher accuracy. In the VMD-BiLSTM diagnostic model, each performance index can exceed 97.3%. This model performs better than VMD-LSTM, BiLSTM, and LSTM models and realizes intelligent classification under four signal conditions of the scarifying tooth harrow: no load, normal operation, mild overload, and serious overload. The proposed method provides great significances for improving the intelligence and technical monitoring levels of residual film collectors and provides a reference for follow-up R&D of intelligent residual film collectors.

Keywords: Roller-type residual film collector; Scarifying tooth harrow; Working condition identification

1. Introduction

During the operation of a roller-type residual film collector, the most critical component, the scarifying tooth harrow, bears the largest force, including the ground supporting surface and soil resistance, among all the components of the entire machine. The normal operation of the scarifying tooth harrow directly affects the follow-up work and film collection efficiency of the machine. Hence, stress–strain monitoring of the scarifying tooth harrow is necessary because it alerts the driver when the machine works abnormally. Traditionally, the faults in residual film collectors are diagnosed and identified based on the experience of the driver [1]. Accurately judging the fault type is difficult, and due to complicated field operation procedures, the agricultural machinery fails to identify the fault through simple detection methods. This situation has resulted in stringent requirements on the accuracy and timeliness of the fault diagnosis of residual film collectors.

In actual strain measurement, strain signals are nonlinear and nonstationary and have a large amount of noise because of the complex operating environment. So it is difficult to accurately identify the earth heaping phenomenon of the scarifying tooth harrow from these signals.With the rapid development of sensor, monitoring, and diagnosis technologies, intelligent fault diagnosis based on multisensor information fusion has elicited extensive interest and has been widely studied [2]. Existing studies have proposed the remote distributed agricultural machinery fault diagnosis system [3] and the constraint-based clogging identification algorithm [4] and have analyzed fault types and phenomena by training based on deep learning [5]. Fault diagnosis and load feedback control systems have been designed , and mechanical analysis and fault diagnosis have been conducted via stacked denoising autoencoders [6], random forest, and support vector machines [7,8]. Existing research shows that most monitoring systems remain at the test stage and cannot be promoted and applied in large areas. At present, fault diagnosis of residual film collectors is being increasingly investigated. Despite the ability to acquire the monitoring information of working conditions, existing fault diagnosis systems still have low fault diagnosis and identification accuracies and exhibit minimal output subordinate feedback and application after the fault diagnosis of agricultural machinery [9]. In addition, the intelligent development of residual film collectors is slow, monitoring systems have been rarely studied, and how to fuse multiple sensors and transmit monitoring data in a real-time accurate manner remains to be further explored.

*E-mail address: 286409568@qq.com
ISSN: 1791-2377
doi:10.25103/jestr.172.08

Given the earth heaping situation of the scarifying tooth harrow of a roller-type residual film collector, three monitoring points were set in the current study, variational mode decomposition (VMD) parameters were optimized via the arithmetic optimization algorithm (AOA), and the reconstructed signal after VMD decomposition was subjected to two-way updating and recursion to establish a fault diagnosis model. Next, the effectiveness and accuracy of the model were verified through datasets to provide an experimental basis for further research on the intelligent development of roller-type residual film collectors.

2. State of the Art

Given the complex transmission, numerous mechanical structures, and poor working conditions of residual film collectors, serious clogging accidents occur; these accidents affect the normal operation of the machines and cause economic losses to farmers. The key components, such as film pick-up roller, scarifying tooth harrow, and stripping roller, of residual film collectors are prone to failure during the working process. Traditionally, faults are judged mainly by experience or addressed only after their occurrence. Intelligent analysis methods for the fault diagnosis of residual film collectors are lacking. Late-stage operation and maintenance can be supported by appropriate agricultural machinery monitoring and diagnostic methods to solve this problem. Jaumann et al. [10] proposed two deep learning models for intelligent condition monitoring of disc mowers to inform the machine operator when a fault occurs. Da et al. [11] from Saint Paul University in Brazil used six dual-plate differential impact sensors to form an array for measuring the grain yield, and their approach effectively reduces the noise interference caused by vibration. Virk et al. [12] reported that variable sowing based on a prescription map can realize variable sowing regulation in accordance with the differences in the nutrients and geographical locations of planting environments; the approach results in reduced costs and increased production. Mouzen et al. [13] designed a depth monitoring system to measure soil compactness online. This system, which combines a balance wheel and a displacement sensor, can reflect the change in tillage depth at high speeds. In the abovementioned studies, the status parameters of machines were intelligently monitored via sensor and information processing technologies, so agricultural machinery has developed toward intelligent and automated directions. China's agricultural machinery monitoring systems developed late, but considerable progress has been achieved in the operating status monitoring and fault diagnosis of different agricultural machineries, and specific breakthroughs have been achieved. However, the developed monitoring devices have poor adaptability and stability. Zhang et al. [14] designed a monitoring system for the feed of a combined harvester that consists of three parts: vehicle terminal, mobile terminal, and information perception module. The system can obtain the feed information of the combined harvester during operation in an accurate, real-time manner, but the system is noisy, and the harvester operates unstably. Yin et al. [15] proposed a tillage depth detection method based on attitude estimation of a subsoiling unit. The system can collect information on tillage depth, operation speed, position, and course in real time, but system tillage depth detection via field experiments still has errors. Xia et al. [16] presented a method of monitoring the tillage depth in real time by using angular-displacement and tilt sensors to solve the poor surface flatness and unstable tillage depth caused by machine rolling. The results showed that the system accuracy is high. Zhou et al. [17] studied a set of field operation monitoring systems for a chain-rake residual film collector, which sends an alarm when an overload fault occurs in the machine and monitors the operating area.

The abovementioned monitoring systems are mainly used in combined harvesters and seeders, but they have high working requirements and low diagnostic accuracy during fault diagnosis. At present, the techniques for residual film collectors, especially for the monitoring and identification of different working conditions for the scarifying tooth harrow of residual film collectors, are lacking. In this study, the reconstructed signal from three monitoring points after VMD decomposition was subjected to two-way updating and recursion with bidirectional long short-term memory (BiLSTM) as the core of the model. Then, iterative training was performed under four working conditions (no load, normal operation, mild overload, and serious overload) of the scarifying tooth harrow to realize the intelligent classification of the four working condition signals. This study is crucial for improving the intelligent and technical monitoring levels of residual film collectors in China and can be used as a reference for subsequent R&D of intelligent residual film collectors.

The remainder of this study is organized as follows: In Section III, the basic algorithm principle and the selection of detection points are briefly introduced, and fault diagnosis models are established. In Section IV, the dataset is imported into BiLSTM and long short-term memory (LSTM) deep learning models to acquire an improved training model, followed by a comparative analysis of the training results obtained through VMD-BiLSTM, VMD-LSTM, BiLSTM, and LSTM models. Then, the accuracy and loss value curves of the four diagnosis models are obtained, the models are verified, and a confusion matrix is generated. In Section V, the study results are summarized, and relevant conclusions are presented.

3. Methodology

3.1 Selection of monitoring points for the scarifying tooth harrow

When the machine operates normally, the scarifying tooth harrow performs scarification forward at a uniform speed, and the scarifying tooth is inserted 80 mm beneath the ground surface to bear soil resistance and the supporting force formed by the soil. The weight of the entire machine is 2 t, and 80% of the force acts on the scarifying teeth during the operation of this machine. Thus, the counterforce of the gravity of the machine applied on the scarifying teeth is 16 *k*N. The total number of the scarifying teeth is 11, each of which bears a supporting force of 1,454 N. The specific soil resistance is 60 *k*Pa. The soil resistance, F, borne by the scarifying teeth can be solved with the calculation formula of specific soil resistance as follows:

$$K = \frac{F}{\eta a b} \tag{1}$$

where K is the specific soil resistance in *k*Pa; η stands for ploughing efficiency, which has a value of 0.7; a is the tillage depth of a single buried component in m; and b is the

single-furrow breadth in m. $F = 0.0672$ *k*N is calculated with $K = 60$ *k*Pa, $a = 0.08$ m, and $b = 0.02$ m.

In this study, the scarifying tooth harrow was subjected to a static characteristic analysis through ANSYS. Q235 ordinary carbon steel was applied as a constraint to the endplates on both sides of the cross beam. Supporting force and soil resistance were applied to the tip of the scarifying teeth, as shown in Fig. 1.

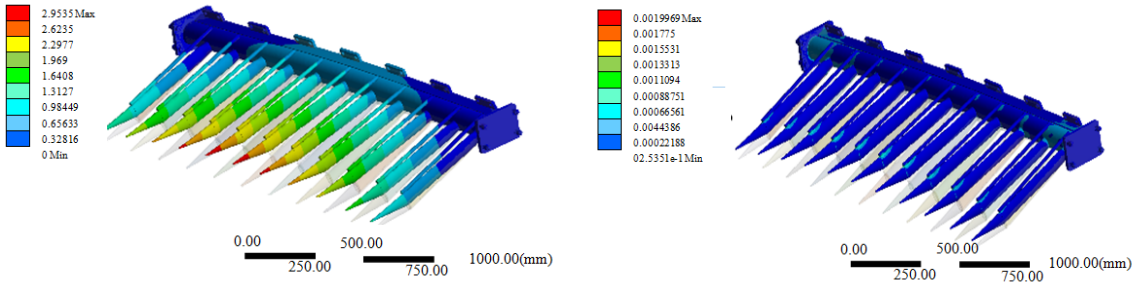

a. Maximum deformation

b. Transient strain cloud picture

Fig. 1. Static analysis of the scarifying tooth harrow

The figure indicates that under the normal working condition, the largest deformation was at the tip of the scarifying teeth, and the maximum transient strain was at the junction between the cross beam and connecting plates on both sides, which was a strain-sensitive site. The pre-experiment showed that the operating condition of the scarifying teeth could be effectively reflected if the strain gauge was placed at the junction between the middle of the cross beam of the scarifying tooth harrow and the two sides. Hence, the three monitoring points were distributed, as shown in Fig. 2.

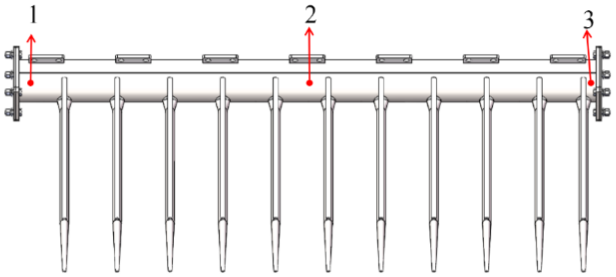

Fig. 2. Schematic of scarifying tooth monitoring locations

3.2 Basic algorithm principle

AOA is a metaheuristic optimization algorithm proposed in 2021 to achieve global optimization in accordance with the distribution characteristics of arithmetic operators [18, 19]. The algorithm steps are as follows:

(1) Search stage: $r_1 > \text{MOA}$ indicates the global search stage, and $r_1 < \text{MOA}$ represents the local development stage. r_1 is a random number between 0 and 1. The calculation equation is as follows:

$$MOA(t) = Min + t \cdot \frac{(Max - Min)}{T} \tag{2}$$

where *Max* and *Min* represent the maximum and minimum values of the acceleration function (1 and 0.2), respectively; t is the current number of iterations; and T stands for the total number of iterations.

(2) Exploration stage: Global exploration is realized through multiplication and division operations. When $r_2 < 0.5$, the division operation-based exploration strategy is executed; and when $r_2 \geq 0.5$, the multiplication operation-based exploration strategy is implemented. The calculation equation is as follows:

$$X(t+1) = \begin{cases} \dfrac{X_b(t)}{MOP + \varphi} \cdot ((UB - LB) \cdot c + LB), r_2 < 0.5 \\ X_b(t) \cdot MOP \cdot ((UB - LB) \cdot c + LB), r_2 \geq 0.5 \end{cases} \tag{3}$$

where $r_2 \in [0,1]$; c is the control parameter of the search process and has a value of 0.499; and φ is the minimal value. The probability calculation formula of the mathematical optimizer is as follows:

$$MOP(t) = 1 - \frac{t^{\frac{1}{\alpha}}}{T^{\frac{1}{\alpha}}} \tag{4}$$

where α is a sensitive parameter that defines the local development accuracy during the iteration, and it has a value of 5.

(3) Development stage: Local development is realized through addition and subtraction. It is formulated by the following equation:

$$X(t+1) = \begin{cases} X_b(t) - MOP \cdot ((UB - LB) \cdot c + LB), r_3 < 0.5 \\ X_b(t) + MOP \cdot ((UB - LB) \cdot c + LB), r_3 \geq 0.5 \end{cases} \tag{5}$$

where $r_3 \in [0,1]$.

VMD is a process of decomposing signal $f(t)$ into a series of intrinsic mode function (IMF) components via Wiener filtering, Hilbert transform, and frequency mixing. The original signal $f(t)$ is decomposed into k IMF components by constructing and solving the constrained variation problem, and penalty factor α, namely, the Lagrange multiplier, is introduced to transform the constrained variation problem into an unconstrained variation problem [20,21]. k and α are two key parameters in VMD.

BiLSTM is a combination of two LSTMs with different directions [22]. LSTM consists of three special structural gates, namely, forget, input, and output, and implements information transmission by using specific tanh network layers, as indicated in Literature [23]. In the current study, the signal reconstructed from the stress – strain signal of the scarifying tooth harrow after VMD was subjected to two-way updating and recursion, followed by iterative training under four working conditions of the scarifying teeth. The BiLSTM network structure is shown in Fig. 3.

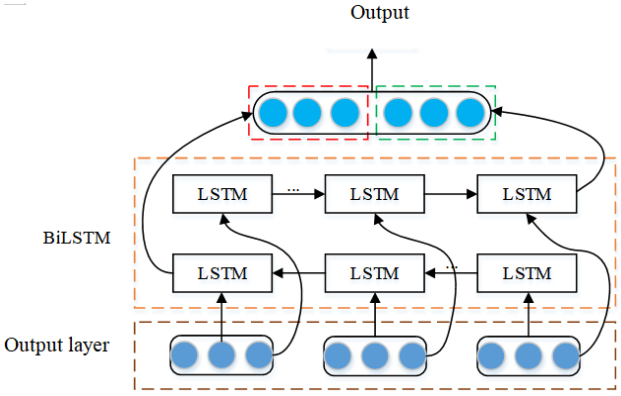

Fig. 3. BiLSTM structure

We defined the operation of states in the following way:

$$\vec{C}_t = LSTM(x_t, \vec{h}_t - 1, \vec{C}_t - 1) \tag{6}$$

$$\bar{C}_t = LSTM(x_t, \bar{h}_t - 1, \bar{C}_t - 1) \tag{7}$$

$$C_t = W^{\mathrm{T}}\vec{C}_t + W^{\mathrm{V}}\bar{C}_t \tag{8}$$

where $\vec{C}_t$ and $\bar{C}_t$ denote the memory cell states of forward and backward LSTMs at time t, respectively, and W^{T} and W^{V} represent the weight coefficients of the forward and backward matrix unit states, respectively.

In this study, the reconstructed signal for the three monitoring points after VMD was subjected to two-way updating and recursion with BiLSTM as the core of the model. Next, iterative training was performed under four working conditions of the scarifying tooth harrow.

3.3 Establishment of fault diagnosis models

(1) Optimization of VMD parameters through AOA

Location updating was implemented for the VMD parameters [k, α] by using AOA. With the minimum value of envelope entropy as the fitness function, the modal number (k) and penalty factor (α) of VMD suitable for the signals at different monitoring points were calculated through optimization. After repeated experiments, the population size was set to 100, the number of iterations was set to 20, the lower boundary was set to [0, 1], and the upper boundary was set to [3600,10].

(2) Working condition identification model (AOA-VMD-BiLSTM) for the scarifying tooth harrow.

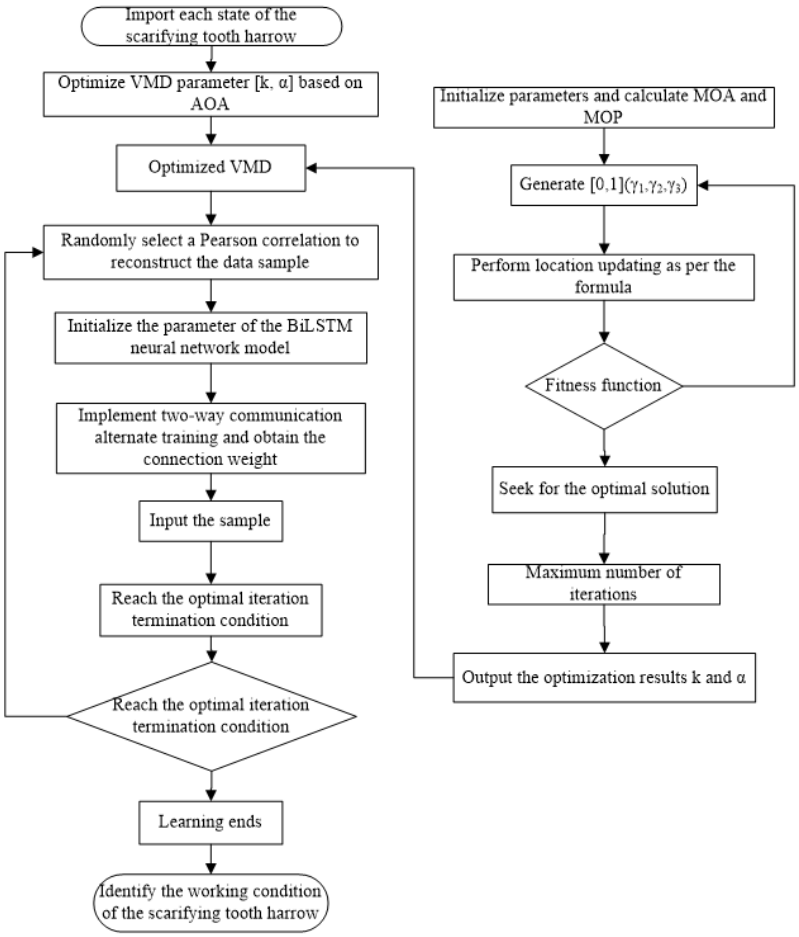

Fig. 4. Working condition identification flowchart

The flowchart of the working condition identification model is displayed in Fig. 4. The specific steps are as follows:

Step 1) Different working conditions were simulated. The strain signals at the three monitoring points on the scarifying tooth harrow were collected by a DH5922N dynamic signal testing analyzer, and the algebraic value of strain was converted into a strain value to obtain the sample signal.

Step 2) The k and α values optimized through AOA were selected, and the signal $f(t)$ at the three monitoring points under different states of the scarifying tooth harrow was decomposed into 3k stable signal IMF components with different characteristics via optimized VMD.

Step 3) The threshold was set. The m IMF components strongly correlated with the original signal at each monitoring point were subjected to signal reconstruction in accordance with the Pearson coefficient to form a new sample dataset, which was divided into training and test sets.

Step 4) A BiLSTM model was constructed, and the training data were inputted. A model with improved performance was acquired by parameter adjustment.

Step 5) The effectiveness and accuracy of the AOA-VMD-BiLSTM model for the scarifying tooth harrow were verified using the dataset.

4. Result Analysis and Discussion

4.1 Data processing under different working conditions of the scarifying tooth harrow

The signal was denoised, and the VMD parameters were optimized by AOA with envelope entropy as the fitness function to effectively classify the working conditions of the scarifying tooth harrow. After optimization, the optimal parameter combinations of the three monitoring points were obtained, as shown in Table 1.

Table 1. Optimal parameter combinations

Optimal parameter	*k*	*α*
Monitoring point 1	7	3,465.5404
Monitoring point 2	3	345.7084
Monitoring point 3	7	3,122.1502

The optimal parameter combination was substituted into VMD, the signals of the three monitoring points were decomposed into a series of stable signal IMF components with different characteristics, and the stress and strain signals at monitoring point 3 were analyzed, as shown in Fig.5. Next, the correlation degree with the original signal of the corresponding monitoring point was calculated through the Pearson correlation coefficient method, the threshold value was set to 0.8, and the signal of the strongly correlated IMF component was reconstructed, as shown in Fig. 6. The reconstructed signal of the serious overload signal at monitoring point 3 had evident frequency characteristics, indicating that the noise part of the data was removed through the reconstruction of the strongly correlated IMF component, and the operating state characteristics of the scarifying tooth harrow were preserved.

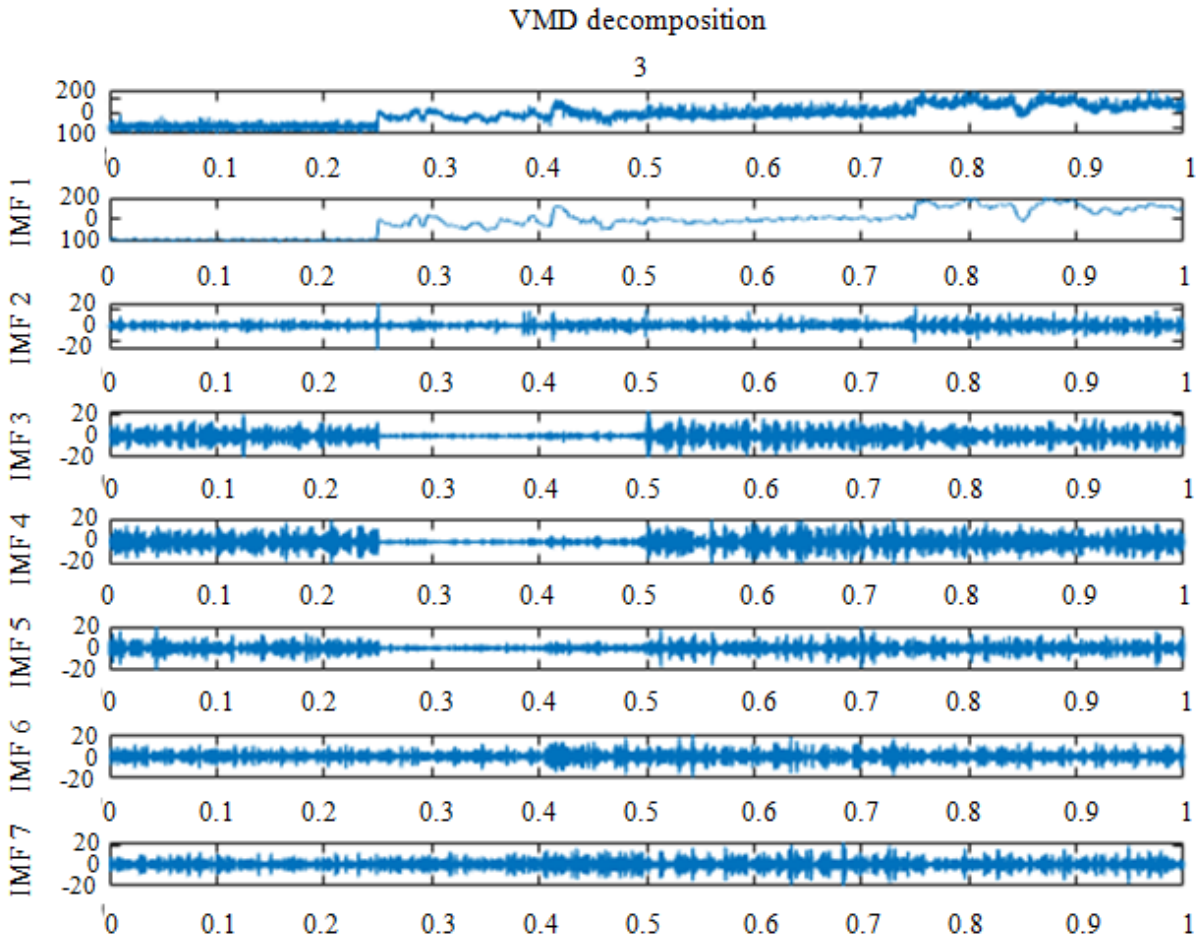

Fig. 5. Signal IMF component of Channel 3

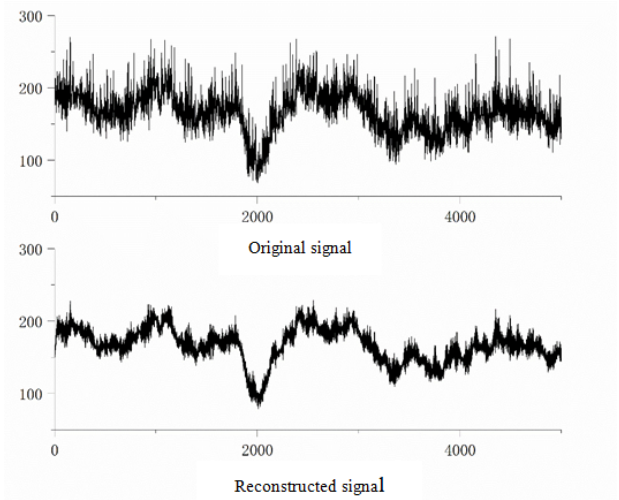

Fig. 6. Comparison of the situation before and after the serious overload signal at monitoring point 3

Excel files were created for the data of each state, and 5,000 nonrepetitive data points were evenly obtained from each monitoring point in a continuous time range. Therefore, the original data of each state contained 15,000 original data points, and the data points did not change after reconstruction. The new sample dataset in the four states contained 4 × 3 × 5,000 = 60,000 data points, the data were labeled, and all samples were dislocated and divided into training and test sets at a proportion of 7:3. The dataset grouping is shown in Table 2.

Table 2. Dataset grouping

Working conditions of the scarifying tooth harrow	Dataset		Label
	Training set	Test set	
No load	10,500	4,500	1
Normal operation	10,500	4,500	2
Mild overload	10,500	4,500	3
Serious overload	10,500	4,500	4

4.2 Data and analysis of four diagnosis models

The new sample set and the original dataset were respectively imported into BiLSTM and LSTM deep learning models for training to acquire an improved training model. The training results of VMD-BiLSTM, VMD-LSTM, BiLSTM, and LSTM models were comparatively analyzed. After 50 iterations, the accuracy and loss value curves of the four fault diagnosis models were obtained as the experimental output results, as shown in Fig. 7

.

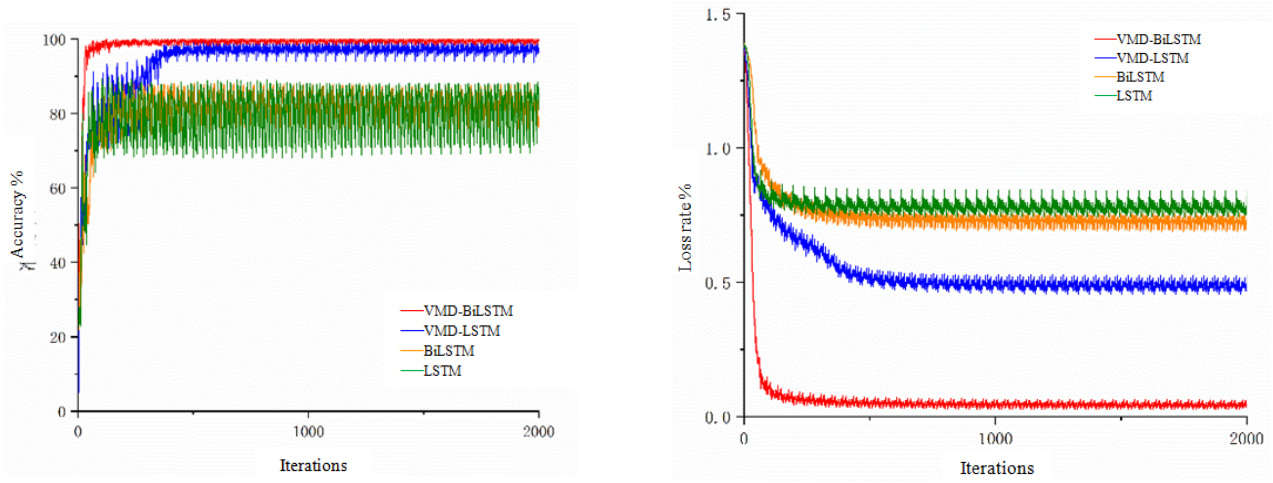

a. Accuracy curve

b. Loss value curve

Fig. 7. Training results

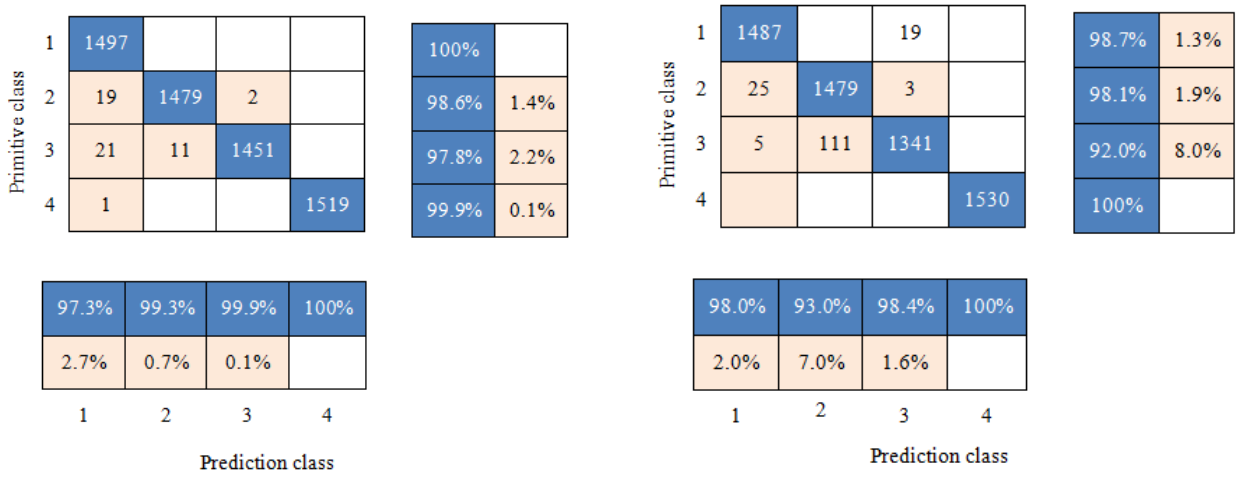

a. VMD-BILSTMB

b. VMD_LSTM

Fig. 8. Confusion matrix of VMD-BiLSTM and VMD-LSTM models

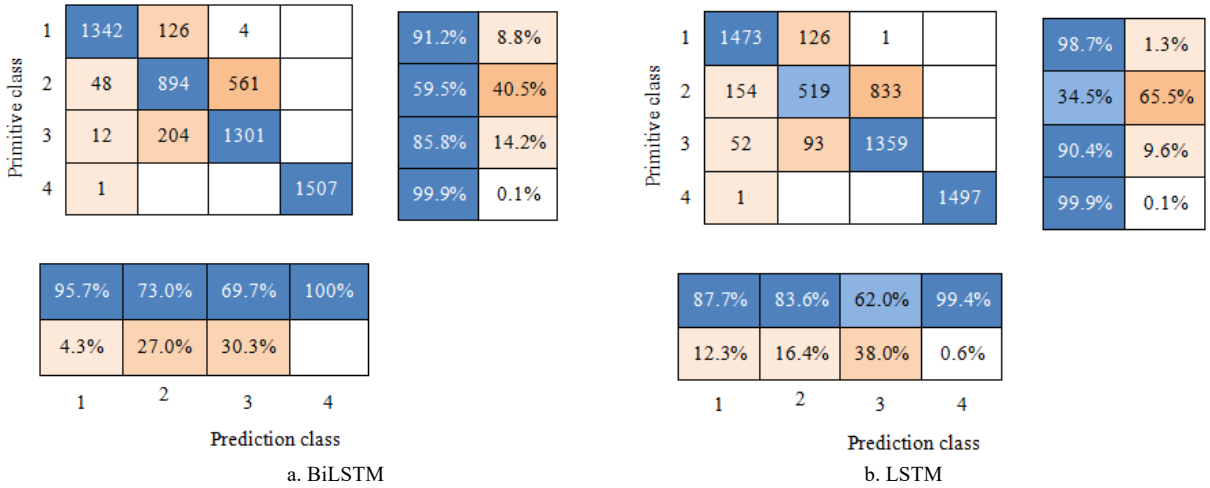

a. BiLSTM b. LSTM

Fig. 9. Confusion matrix of BiLSTM and LSTM models

Fig.7(a) indicates that initially, the VMD-BiLSTM model converged and iterated rapidly. After 200 training iterations, the accuracy curve gradually stabilized and reached a high value. Before 500 training iterations, the VMD-LSTM model converged slowly. Its accuracy fluctuated considerably, stabilized, and fluctuated again within small values. The LSTM and BiLSTM neural network models experienced serious dispersion after 150 training iterations, and their accuracy was unstable and fluctuated considerably, which affected the judgement results substantially. The convergence effect did not improve even after 2,000 iterations. The accuracy of the BiLSTM neural network model was higher than that of the LSTM model and had smaller fluctuations.

The training results of the four neural network models in Fig.7(b) indicate that the four models became stable after 500 training iterations. After 200 training iterations, the loss value of the VMD-BiLSTM model reached zero, and the convergence result was stable. The VMD-LSTM model converged slowly and exhibited stability only after 500 training iterations; its loss value was large and fluctuated around 0.5. The loss values of the BiLSTM and LSTM models were approximate and much greater than those of the two other models, leading to reduced accuracy.

In summary, the VMD-BiLSTM and VMD-LSTM models performed well in processing complex signals, and the former had a higher convergence rate, better convergence stability, and higher accuracy than the latter. The dataset was inputted into the four models, and a confusion matrix was generated to verify that the models could reflect the working condition of the scarifying tooth harrow comprehensively.

Fig.8 shows that the overall accuracy of the training result obtained by VMD-BiLSTM was 99.1%. After the same dataset was imported, the overall accuracy of the training result of the VMD-LSTM model became 97.3%. On the basis of the results, this model was subjected to incomplete identification under normal operation and mild soil heaping conditions, and its effect was slightly poorer than that of the VMD-BiLSTM model.

As shown in Fig. 9, the overall accuracies of the training results of the BiLSTM and LSTM models were 84.5% and 80.8%, respectively. The identification effect of LSTM under the mild-overload condition was poorer than that under normal operation. Moreover, 65.5% of the data were identified under no-load and mild-load conditions, and the proportion of data identified under the mild-overload condition was large.

The four confusion matrix diagrams indicate that the identification accuracy of the proposed diagnosis model for the operating status of the scarifying tooth harrow was elevated substantially, indicating a good working condition identification performance.

The training results obtained by the four diagnosis models regarding the different working condition data of the scarifying tooth harrow were comparatively analyzed using the same dataset, as indicated in Table 3. Each performance index of the VMD-BiLSTM diagnosis model exceeded 97.3% and was better than those of the three other models. The model realized the intelligent classification of the no-load, normal-operation, mild-overload, and serious-overload signals of the scarifying tooth harrow.

Table 3. Index comparison of the different models

Evaluation index	VMD-BiLSTM	VMD-LSTM	BiLSTM	LSTM
Accuracy (%)	99.1	97.5	84.1	80.8
Precision (%)	97.3	98.1	95.7	87.7
Recall (%)	99.8	98.7	91.2	98.7
Harmonic average (%)	98.6	98.4	93.4	92.8

5. Conclusions

In actual strain measurement, the strain signal is nonlinear and nonstationary with abundant noise due to the complex operating environment, so accurately identifying the soil heaping phenomenon of the scarifying tooth harrow is difficult. In this study, the AOA-VMD-BiLSTM model was proposed to identify the working condition of the scarifying tooth harrow. After iterative training under four working conditions, the following conclusions were obtained.

(1) AOA can obtain the optimal parameter combination for the three monitoring points of the scarifying tooth harrow after signal denoising and optimization on the basis of the optimized VMD parameters.

(2) The accuracy and loss value curves of the VMD-BiLSTM, VMD-LSTM, BiLSTM, and LSTM models are acquired by comparatively analyzing the training results of the four fault diagnosis models. The results reveal that among the four models, VMD-BiLSTM processes the complex signals the best, with faster convergence, better convergence stability, and higher accuracy.

(3) The processing effect and accuracy of VMD-BiLSTM exceeds 97.3%, and VMD-BiLSTM is superior to VMD-LSTM, BiLSTM, and LSTM. The model realizes the intelligent classification of the no-load, normal-operation, mild-overload, and serious-overload signals of the scarifying tooth harrow.

In this study, theory is combined with simulation experiments, and the field experiments are reduced while still ensuring the dynamic performance of the system. The experiment cost is also reduced. This study caters to the networking development needs of mechanical intelligence systems and has high practical importance. However, the interference of factors in real experiments should be further considered if the proposed optimization algorithm is adopted. In future research, high-performance processors may be employed to perform real-time identification of working conditions by using algorithm models to achieve stable results.

Acknowledgements

The authors are grateful for the support provided by National Natural Science Foundation of China (Grant No. 52365038).

References

[1] M. Hakim, A. B. Omran, A. N. Ahmed, M. Al-Waily, and A. Abdallatif, "A systematic review of rolling bearing fault diagnoses based on deep learning and transfer learning: Taxonomy, overview, application, open challenges, weaknesses and recommendations," *Ain. Shans. Eng. J.,* vol. 14, no. 4, Apr. 2023, Art.no. 101945.

[2] Z. M. Qiu, G. X. Shi, B. Zhao, X. Jin, and L. M. Zhou, "Combine harvester remote monitoring system based on multi-source information fusion," *Comput. Electron. Agr.,* vol. 194, Mar. 2022, Art.no. 106771.

[3] P. F. Sun and Y. He, "Study on Remote Distributed Fault Diagnosis System in Modern Agricultural Machinery," *Adv. Mater. Res.,* vols. 225-226, pp. 356-359, Apr. 2011, doi: 10.4028/www.scientific.net/ AMR. 225-226.356.

[4] R. Q. Zhao, J. Fu, Z. Chen, L. Tian, and L. Q. Ren, "Low-rank-constraint-based machine vision algorithm for chaffer-sieve-clogging recognition of corn harvester," *Comput. Electron. Agr.,* vol. 198, Jul. 2022, Art.no. 107056.

[5] L. J. Wu, R. Xia, H. Y. Zhan, and X. Y. Han, "Fault Prediction Technology Based on Deep Learning," (in Chinese), *Comput. Meas.Control.,* vol. 26, no. 2, pp. 9-12, Feb. 2018.

[6] C. B. Xi, G. Y. Yang, L. Liu, J. liu, X. H. Chen, and Z. Y. Ma, "Operation faults monitoring of combine harvester based on SDAE-BP,"(in Chinese), *Trans. Chin. Soc. Agr. Mach*(*Transactions of the CSAM).,* vol. 36, no. 17, pp. 46-53, Sep. 2020.

[7] P. J. García Nieto, E. García-Gonzalo, F. Sánchez Lasheras, and F. J. de cos Juez, "Hybrid PSO – SVM-based method for forecasting of the remaining useful life for aircraft engines and evaluation of its reliability," *Reliab. Eng. Syst. Safe.,* vol. 138, pp. 219-231, Jun. 2015.

[8] X. Zhou, X. C. Xu, J. F. Zhang, L. Wang, D. F. Wang, and P. P. Zhang, "Fault diagnosis of silage harvester based on a modified random forest," *Inform. Process. Agr (IPA).,* vol. 10, no. 3, pp. 301-311, Sep. 2023.

[9] J. Jia and J. J. Lin, "Application of Modern Multimedia and Sensing Technology in Fault Detection and Diagnosis of Hydraulic Agricultural Machinery," *Wirel. Commun. Mob. Com.,* vol. 2022, Sept. 2022, Art.no. 8627554.

[10] M. Jaumann, E. Olcay, and T. Oksanen, "Condition Monitoring using Convolutional Neural Network in Agricultural Machinery - Use Case: Disc Mower," *IFAC-PapersOnLine.*, vol. 55, no. 32, pp. 235-240, Nov. 2022.

[11] G. Wu, M. Z. Li, X. F. An, and J. F. Liu, "Development of an impact-based yield monitor with can-bus," *Sensor. Lett.,* vol. 9, no. 3, pp. 974-980, Jun. 2011.

[12] S. S. Virk, J. P. Fultion, and W. M. Porter, "Row-crop planter performance to support variable-rate seeding of maize," *Precis. Agric.,* vol. 21, no. 3, pp. 603-619, Jun. 2019.

[13] W. Saeys, A. M. Mouazen, J. Anthonis, and H. Ramon, "An automatic depth control system for online measurement of spatial variation in soil compaction, Part 2: Modelling of the depth control system," *Biosyst. Eng*., vol. 3, pp. 89, 2004.

[14] Z. Q. Zhang, Y. F. Sun, R. J. Liu, M. Zhang, H. Li, and M. J. Li, "Design and Test of Feed Rate Monitoring System for Combine Harvester," (in Chinese), *Trans. Chin. Soc. Agr. Mach* (*Transactions of the CSAM).,* vol. 50, no. 6, pp. 85-92, Jun. 2019.

[15] Y. X. Yin, C. Wang, Z. J. Meng, J. P. Chen, S. X. Guo, and W. C. Qin, "Operation Quality Measurement Method for Tilling Depth of Suspended Subsoiler," (in Chinese), *Trans. Chin. Soc. Agr. Mach* (*Transactions of the CSAM).,* vol. 49, no. 4, pp. 68-74, Apr. 2018.

[16] J. F. Xia, D. Li, G. Y. Liu, J. Cheng, K. Zheng, and C. M. Luo, "Design and Test of Electro-hydraulic Monitoring Device for HitchTillage Depth Based on Measurement of Tractor Pitch Angle," (in Chinese), *Trans. Chin. Soc. Agr. Mach* (*Transactions of the CSAM).,* vol . 52, no. 8, pp. 386-395, Aug. 2021.

[17] Y. B. Zhou, "Research on On-line Monitoring System of Chain Rake Type Residual Film Recoverer in Field Operation," M. S. thesis, Dept. Mach. Eng., Xinjiang Agric Univ., Urumqi, China, 2021.

[18] M. A. Zermani, G. Manita, A. Chhabra, E. Feki, and A. Mami, "FPGA-based hardware implementation of chaotic opposition-based arithmetic optimization algorithm," *Comput. Method. Appl. M.,* vol. 154, Mar. 2021, Art.no. 111352.

[19] H. M. Jia, Y. X. Liu, Q. X. Liu, S. Wang, and R. Wang, "Hybrid Algorithm of Slime Mould Algorithm and Arithmetic Optimization Algorithm Based on Random Opposition-Based Learning," *J. Front. Comput. Sci. Technol.,* vol. 16, no. 5, pp. 1182-1192, May. 2022.

[20] Q. Y. Zhou, C. Yi, L. Lei, X. W. Song, D. Xu, and C. G. Huang, "Multi-Objective Sparsity Maximum Mode De-Composition: A New Method for Rotating Machine Fault Diagnosis on High-Speed Train Axle Box," *IEEE T. Signal. Proces.,* vol. 72, no. 10, pp. 12744-12756, Apr. 2023.

[21] X. L. Zhang, X. Wang, Z. K. Xue, Z. Y. Xue, and J. W. Lv, "Fault Diagnosis of Aviation Hydraulic Pipeline Clamp Based on VMD and LSTM Model," (in Chinese), *CHN Hyd. Penu.,* vol. 46, no. 8, pp. 26-33, Aug. 2022.

[22] P. Dhaka and B. Nagpal, "WoM-based deep BiLSTM: smart disease prediction model using WoM-based deep BiLSTM classifier," *Multimed. Tools. Appl.,* vol. 82, pp. 25061-25082, Jan. 2023.

[23] L. L. Zu, P. Z. Liu, Y. P. Zhao,T. H. Li, and H. LI, "Solar Greenhouse Environment Prediction Model Based on SSA-LSTM,"(in Chinese) *Trans. Chin. Soc. Agr. Mach* (*Transactions of the CSAM).,* vol. 23, no. 2, pp. 351-358, Feb. 2023.